High performance relaxor ferroelectric textured ceramics for electrocaloric refrigeration

Xuexin Li[1], Jinglei Li[1*], Yang Li[1], Xuechen Liu[1], Shuai Yang[1], Jie Wu[1], Dingwei Hou[1], Jinjing Zhang[1], Haijun Wu[2], Yang Zhang[3,1], Xiangdong Ding[2], Jun Sun[2], Shujun Zhang[4], Hongliang Du[5]*, Fei Li[1]*

[1]*Electronic Materials Research Laboratory (Key Lab of Education Ministry), State Key Laboratory for Mechanical Behavior of Materials and School of Electronic and Information Engineering, Xi'an Jiaotong University, Xi'an, China*
[2]*State Key Laboratory for Mechanical Behavior of Materials, Xi'an Jiaotong University, Xi'an 710049, China*
[3]*Instrumental Analysis Center of Xi'an Jiaotong University, Xi'an Jiaotong University, Xi'an 710049, China*
[4]*Institute of Superconducting and Electronic Materials, Australian Institute for Innovative Materials, University of Wollongong, Wollongong, NSW, 2500, Australia*
[5]*Multifunctional Electronic Ceramics Laboratory, College of Engineering, Xi'an International University, Xi'an 710077, China*
*Corresponding author: lijinglei@xjtu.edu.cn; duhongliang@126.com; ful5@xjtu.edu.cn

Note 1.ECE measurement

To overcome the challenges of uneven heat distribution during tests, we employ a method called electrocaloric calorimetry, featuring in-situ calibration to tailor measurements of the electrocaloric effect. This approach utilizes a reference electrode, integrated during fabrication via magnetron sputtering, achieving a resistance near 15 ohms. The schematic shows two wires, labeled A and B, connected to the lower electrode of the electrocaloric (EC) sample. The sample is situated on a Heat Flux Sensor (HFS) cushioned by a thermo-conductive gel. A small voltage (V_{Ref}) corresponding to resistance R, is applied through wires A and B, allowing for the accurate computation of reference heat using Joule's law.

$$Q_{Ref} = \int \frac{U^2}{R} dt$$

Further detailing the setup, a digital voltmeter, part of a combined system with a computer and oscilloscope, reads the voltage across the reference electrode precisely. The reference heat(RH) thus generated is detected as an electrical signal by the HFS. By calculating the heat flux signal, the ratio of the sample's heat emission or absorption to the electrical signal area is determined. Subsequently, high voltage (HV) is applied to the EC sample through leads B and C, causing the sample to either release or absorb heat when the HV is toggled on and off. By correlating the EC signal with the reference heat ratio, we can accurately capture the heat response of the sample under specific thermal contact conditions with the sensor.

The quantity of heat absorbed by the EC material (ΔQ) is calculated by integrating the thermal flow curve area. The adiabatic temperature change (ΔT) of the material is then computed using the formula

$$\Delta T = \frac{\Delta Q}{c_E * m}$$

where ΔQ is the heat absorbed, c_E is the material's specific heat capacity and m is the mass of the sample.

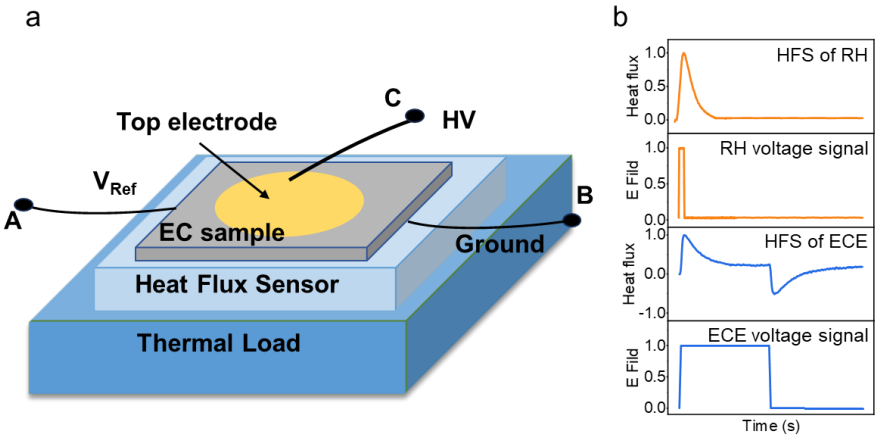

Supplementary Figure 1. (a) Schematic of the measurement set-up; (b) The key signal involved to calibrate the RH and ECE measurement in situ.

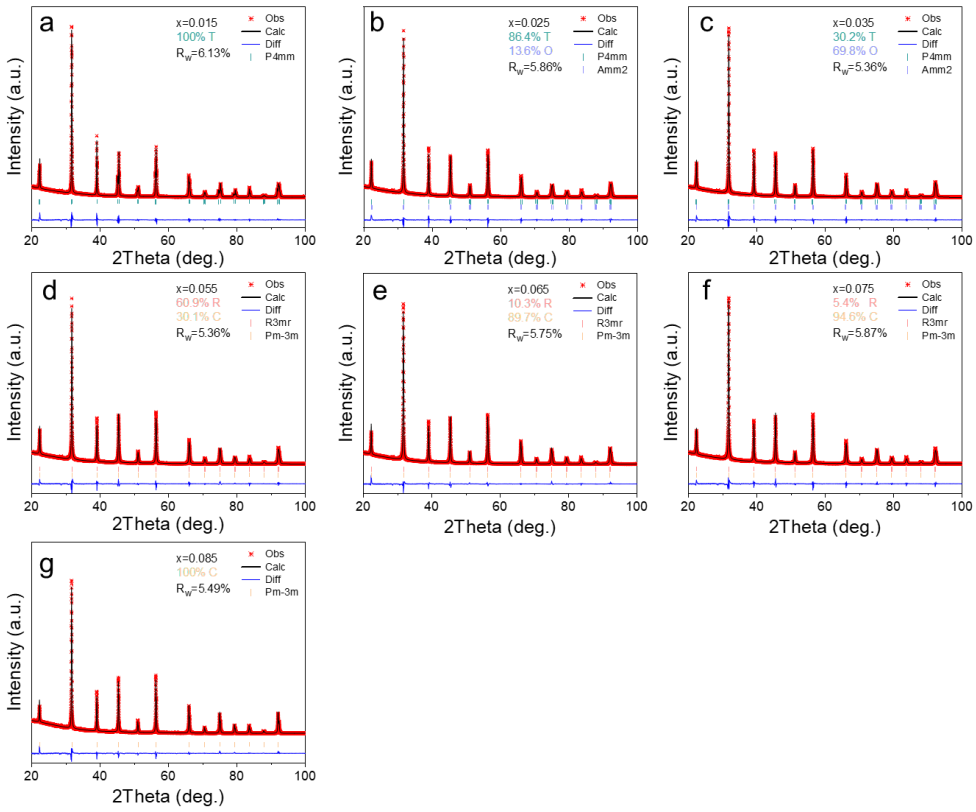

Supplementary Figure 2. Results of X-ray Diffraction (XRD) Rietveld structural refinement for BT-*x*KN(*x*=0.015~0.085) ceramics.

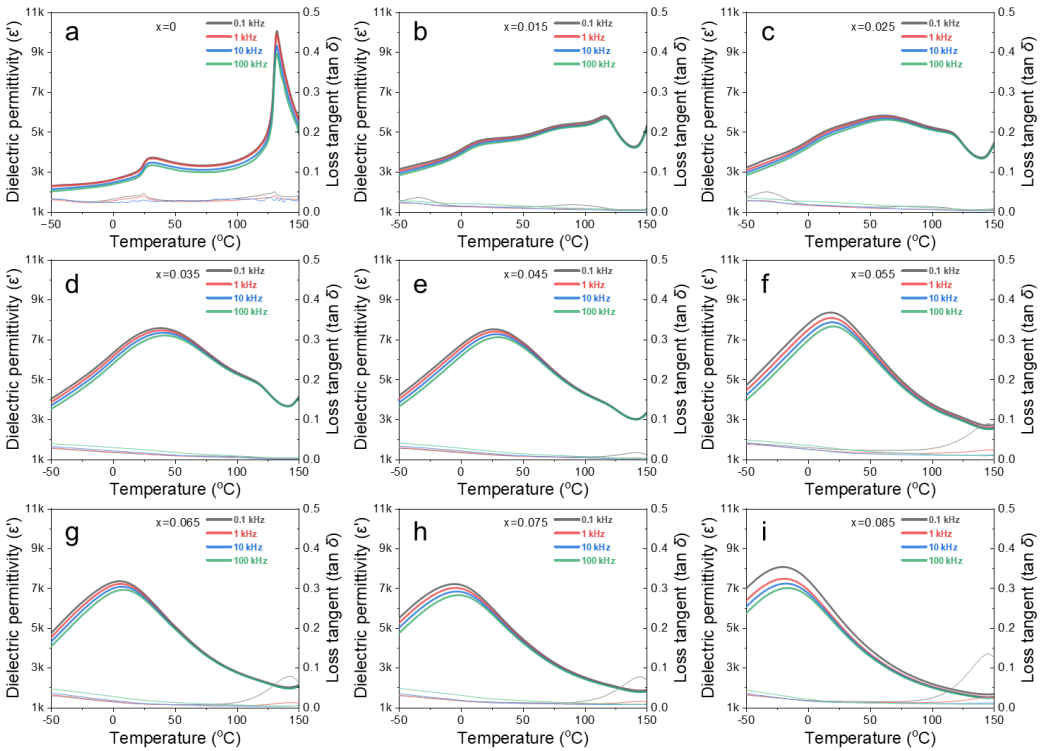

Supplementary Figure 3. Temperature dependence of dielectric properties of BT-*x*KN(*x*=0.015~0.085)

ceramics.

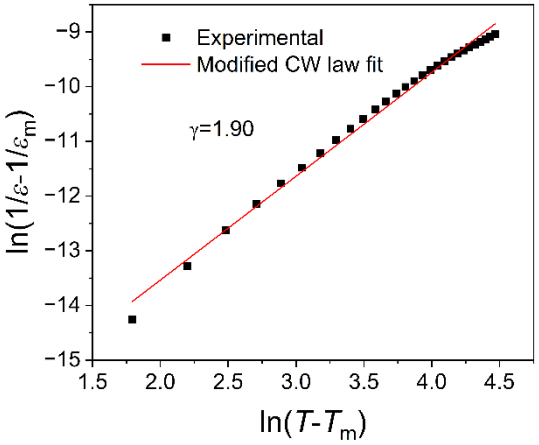

Supplementary Figure 4. Fitting of data from BT-0.045KN ceramics above the transition temperature to the modified Curie-Weiss law

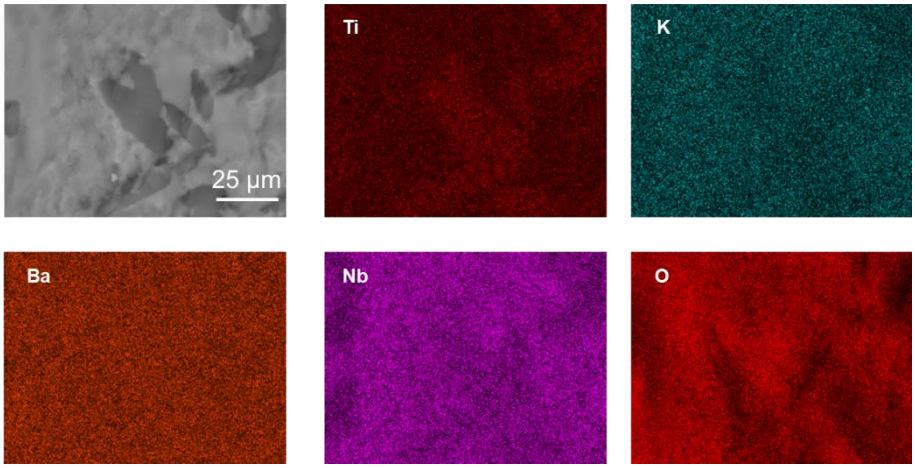

Supplementary Figure 5. The second phase produced during the weaving process of BT-KN ceramics due to potassium volatilization

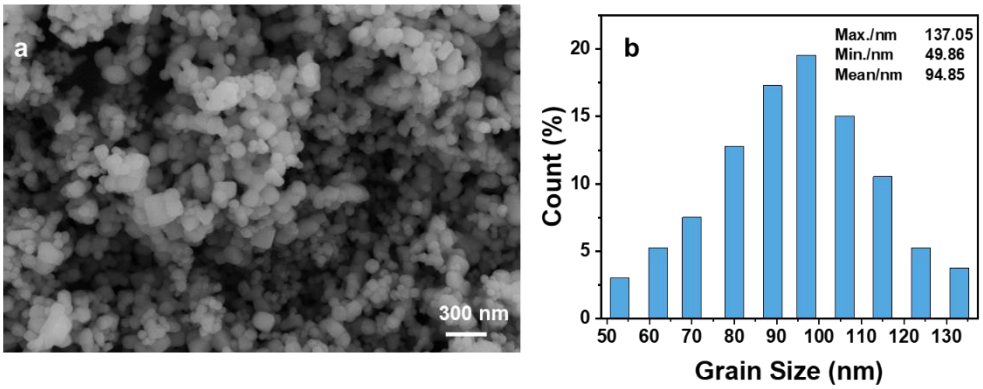

Supplementary Figure 6. (a) Scanning Electron Microscopy image of BT-0.05KN powder morphology after pre-sintering; (b) Particle size distribution statistics.

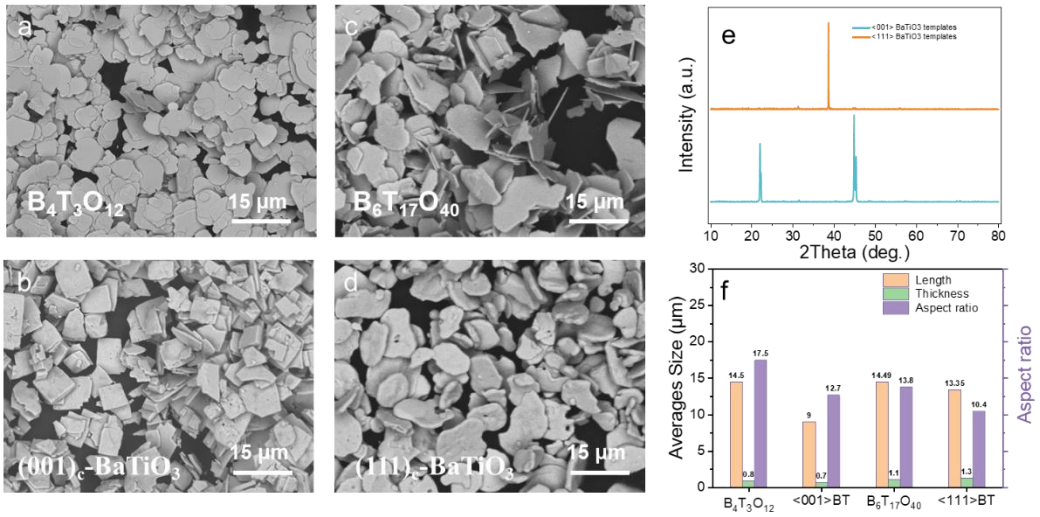

Supplementary Figure 7. Scanning electron microscope images of (a) $B_4T_3O_{12}$, (b) $(001)_c$-$BaTiO_3$; (c) $B_6T_{17}O_{40}$; (d) $(111)_c$-$BaTiO_3$; (e) X-ray diffraction patterns of $(001)_c$-$BaTiO_3$ and $(111)_c$-$BaTiO_3$ templates; (f) aspect ratio distribution.

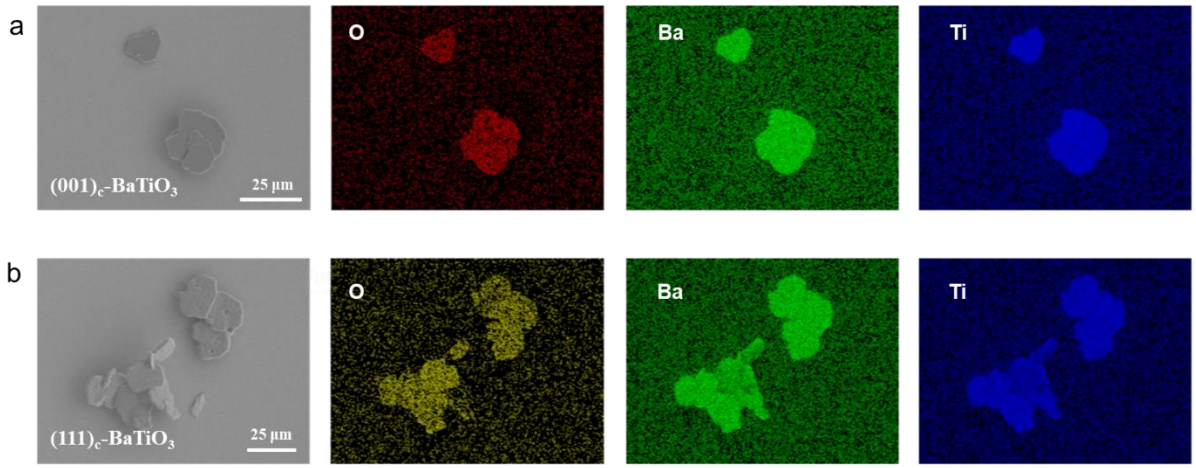

Supplementary Figure 8. Surface morphology and EDS of templates and corresponding precursors: (a) $(001)_c$-$BaTiO_3$; (b) $(111)_c$-$BaTiO_3$.

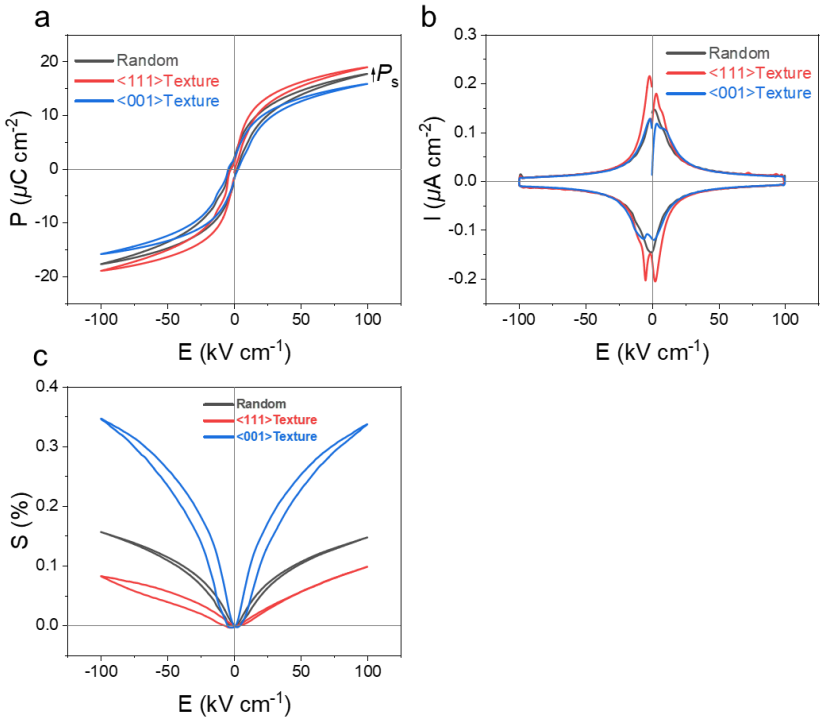

Supplementary Figure 9. (a) *P-E* loops; (b) *I-E* curves and (c) electrostriction properties of Random, $<001>_c$ and $<111>_c$ BT-KN texture ceramics

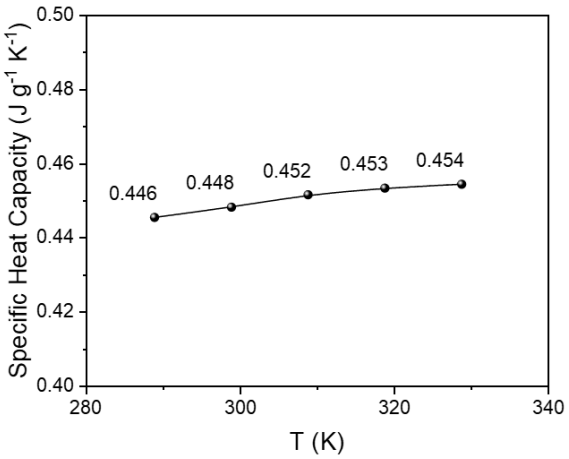

Supplementary Figure S10. Specific heat capacity of BT-45KN ceramics measured during the heating process.

Supplementary Table S1. XRD Rietveld refinement parameters for BT-*x*KN (*x*=0.015~0.085) ceramics.

Sample (%)	Density (g cm^{-3})	Space group	Phase content (%)	a (Å)	b (Å)	c (Å)	α (◦)	β (◦)	γ (◦)	Rw(%)
x=1.5	6.00	P4mm(T)	100	3.9971	3.9971	4.0284	90	90	90	6.13
x=2.5	5.99	P4mm(T)	86.4	4.0011	4.0011	4.0123	90	90	90	5.86
		Amm2(O)	13.6	3.9776	5.7099	5.6793	90	90	90	

x=3.5	5.96	P4mm(T)	30.2	4.0052	4.0052	4.0202	90	90	90	5.36
		Amm2(O)	69.8	3.9989	5.6718	5.6719	90	90	90	
x=4.5	5.95	Amm2(O)	16.7	3.9950	5.6762	5.6887	90	90	90	5.62
		R3m(R)	83.3	4.0084	4.0084	4.0084	89.95	89.95	89.95	
x=5.5	5.94	R3m(R)	60.9	4.0074	4.0074	4.0074	90.01	90.01	90.01	5.36
		Pm-3m(C)	39.1	4.0097	4.0097	4.0097	90	90	90	
x=6.5	5.93	R3m(R)	10.3	4.0157	4.0157	4.0157	89.80	89.80	89.80	5.75
		Pm-3m(C)	89.7	4.0072	4.0072	4.0072	90	90	90	
x=7.5	5.94	R3m(R)	5.4	4.0088	4.0088	4.0088	90.05	90.05	90.05	5.87
		Pm-3m(C)	94.6	4.0055	4.0055	4.0055	90	90	90	
x=8.5	5.89	Pm-3m(C)	100	4.0111	4.0111	4.0111	90	90	90	5.49

Supplementary Table S2. Physical parameters for BT-KN ceramics in the ECE testing.

Sample	Density ($g\ cm^{-3}$)	Active area (mm^2)	Thickness (um)
Random BT-45KN	5.62	12.56	105
$<001>_c$ Texture BT-45KN	5.58	12.56	98
$<111>_c$ Texture BT-45KN	5.64	12.56	112